

Energy-related applications of functional porous metal–organic frameworks*

Shengqian Ma[‡] and Le Meng

Department of Chemistry, University of South Florida, 4202 E. Fowler Avenue, Tampa, FL 33620, USA

Abstract: As a new type of functional materials, porous metal–organic frameworks (MOFs) have experienced tremendous development in the past decade. Their amenability to design, together with the functionalizable nanospace inside their frameworks, has afforded them great potential for various applications. In this review, we provide a brief summary of the current status of porous MOFs in energy-related applications, mainly, energy gas storage, CO₂ capture, gas separation, catalysis, and fuel cells.

Keywords: CO₂ capture; catalysis; energy; fuel cells; gas separation; gas storage; porous metal–organic frameworks.

INTRODUCTION

With the continuous growth of economies and populations around the world as well as the depletion of fossil oil reserves and the increasing threat of global warming, energy has become one of the central issues for human beings in the 21st century [1]. This has given urgency to energy research, prompting the search for alternative energy sources on one hand and urging the development of clean energy technologies on the other [2]. Some significant technical challenges have been recognized as the development of novel functional materials capable of improving energy efficiencies as well as recognizing small molecules for various applications [3]. These issues can be addressed by employing highly porous materials whose nanospace can be engineered with specific functionality [4], and porous metal–organic frameworks (MOFs), which have exceptionally high surface areas as well as functionalizable pore structures, are playing an unusual role in this respect [5].

Porous MOFs represent a new type of porous materials, and they are highly crystalline 3D inorganic–organic hybrids constructed by assembling metal ions or small metal-containing clusters [known as secondary building units (SBUs)] with multidentate organic ligands (such as carboxylates, tetrazolates, sulfonates) via coordination bonds [6]. Due to their superior characteristics and properties, porous MOFs have witnessed explosive development and rapid progress in the past decade [7]. They are amenable to design [8], their pore sizes can be systematically tuned by controlling the length of the organic ligands [9], and, in particular, their pore walls can be functionalized for specific applications via either ligand design [10] or postsynthetic modification [11]. The most intriguing feature of porous MOFs lies in their exceptional surface areas [2], and the record for highest published surface area in porous MOFs has been broken repeatedly over the past several years. For example, a porous MOF with a Langmuir surface area of 4500 m²/g was reported for MOF-177 in 2004 [12]; this value was eclipsed

Pure Appl. Chem.* **83, 1–252 (2011). A collection of invited, peer-reviewed articles by former winners of the IUPAC Prize for Young Chemists, in celebration of the International Year of Chemistry 2011.

[‡]Corresponding author: Tel.: +1 813 974 5297; Fax: +1 813 974 3203; E-mail: sqma@usf.edu

less than one year later by MIL-101, with a Langmuir surface area of 5500 m²/g [13]; the current record is held by MOF-210 which possesses an extremely high Langmuir surface area of over 10000 m²/g [14]. These merits of porous MOFs not only make them stand out from other porous materials, but also push them to the forefront of energy research, which has been particularly driven by the increase of world energy demand as well as the dwindling amount of petroleum oil deposits and escalating threat of global warming. The aim of this review is to briefly summarize recent developments in porous MOFs for energy-related applications, which includes energy gas storage, CO₂ capture, gas separation, catalysis, and fuel cells.

ENERGY GAS STORAGE APPLICATION OF POROUS MOFs

Current storage of energy gases such as hydrogen, methane, and acetylene primarily relies on the utilization of high-pressure tanks and multi-stage compressors, which, however, could cause some safety issues for mobile applications particularly in the case of acetylene gas. One of the challenges for safe and economical use of porous MOFs lies in the development of a viable method to efficiently trap those energy gas molecules in a confined space for various applications [2,6]. Porous MOFs, whose nanospace can serve as the ideal room to accommodate gas molecules, provide great opportunities to address this issue, and the following section will give an overview of the state-of-the-art studies of hydrogen, methane, and acetylene storage in porous MOFs.

Hydrogen storage in porous MOFs

Hydrogen is an ideal clean energy carrier and has some ubiquitous merits. It is carbon-free, and the byproduct after energy release is only water, which in reverse can be an inexhaustible resource for hydrogen. Its high energy density, which can nearly triple that of gasoline per mass unit, together with the more than double efficiency for the performance of fuel cells compared to internal combustion engines, makes hydrogen-powered fuel-cell automobiles very attractive to replace those currently powered by petroleum [2,6,15,16]. However, the extremely low volumetric storage density of hydrogen (0.08 kg/m³ at ambient temperature and pressure) presents a barrier that impedes its practical usage as a fuel for vehicles. To guide the research into hydrogen storage, the U.S. Department of Energy (DOE) has set a number of targets for the on-board hydrogen storage system [17], and recently revised them as: 0.055 kg/kg or 0.040 kg/l by the year 2015, and 0.075 kg/kg or 0.070 kg/l as the ultimate values [18].

Owing to their superior merits of exceptionally high surface areas, tunable pore sizes, functionalizable pore walls, and well-defined hydrogen–framework interacting sites, porous MOFs have recently been intensively explored as a promising candidate to approach DOE targets for on-board hydrogen storage [2,6]. Since the first report of hydrogen adsorption on a porous MOF in 2003 [19], over 200 porous MOFs have been investigated for hydrogen storage, and they have demonstrated superior performances compared to other porous materials [2]. Several authoritative review articles for this topic have appeared [20–23], so rather than being exhaustive, we will just briefly summarize some strategies that have been employed to enhance hydrogen storage capacities in porous MOFs.

One fascinating feature of porous MOFs is their high crystallinity, which affords the probability to identify the hydrogen adsorption sites as well as to elucidate the hydrogen–framework interactions either through computation methods [24] or via experimental tools [2,23]. In terms of experimental tools, neutron-based techniques are the most powerful for hydrogen research, due to the fact that hydrogen has a very large neutron cross-section [15,23]. For detailed understanding of the location of H₂ and the energetics of H₂–framework interactions within porous MOFs, one can turn to neutron diffraction and inelastic neutron scattering (INS), respectively [2]. Recent neutron powder diffraction studies on porous MOFs have identified metal centers, particularly, unsaturated metal centers (UMCs), as the first

occupied sites with relatively high energy for hydrogen molecules, and the successive occupying sites associated with the organic linkers which usually account for the large portion of hydrogen adsorption [25–28]. INS studies on the same materials have drawn a similar conclusion that the hydrogen molecules occupy the sites around the metal-cluster centers first with remaining sites occupied progressively around the organic ligands [19]. In addition to identifying the discrete hydrogen-binding sites, INS can provide very useful information on the energetics of H₂–framework interactions in porous MOFs. Recent INS studies have revealed that the metal centers have higher hydrogen-binding energy than the organic linkers [29–31], and the H₂–framework interactions of the interpenetrating porous MOFs are stronger compared to the non-interpenetrating counterparts [32]. These neutron-based studies not only provide clear pictures for understanding hydrogen adsorption in porous MOFs, but also lay a foundation for the rational design of new porous MOF materials with high hydrogen storage capacities.

For hydrogen storage in porous MOFs, two conditions have been usually studied: one is at 77 K/1 atm, and the other is under high pressure at 77 K or ambient temperatures [21]. As for hydrogen storage at 77 K/1 atm, the capacities are affected by surface area/pore volume, pore sizes, interpenetration, ligand functionalization, and UMCs, etc.; as for hydrogen storage under high pressure, high surface area and high hydrogen affinity usually favor high hydrogen uptakes [6].

Although the U.S. DOE targets for hydrogen storage are set at the condition of near-ambient temperatures and high pressures, great efforts have been dedicated to the exploration of various strategies to enhance hydrogen uptakes in porous MOFs at 77 K/1 atm, and these studies can be very useful and instructive at this early stage of exploration for hydrogen storage materials [2,6].

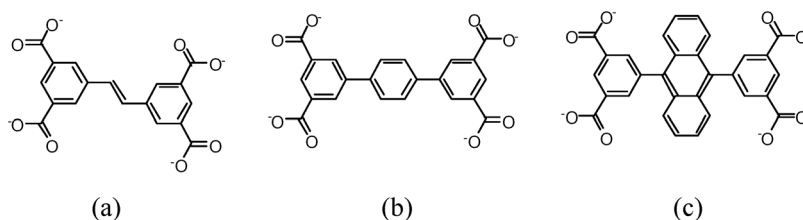
The influence of surface area and pore volume on hydrogen uptake at 77 K/1 atm has been widely investigated in porous MOFs; however, it has been found that for porous MOFs with high surface areas (above 1000 m²/g) and large pore volumes (over 1.0 cm³/g), there is no direct correlation between surface area/pore volume and hydrogen adsorption [6,15,16]. For example, MOF-177 can only adsorb 1.25 wt % hydrogen at 77 K/1 atm, despite its high surface area of 4500 m²/g and pore volume of 1.61 cm³/g; however, IRMOF-8, whose surface area (1466 m²/g) and pore volume (0.52 cm³/g) are less than one-third of those of MOF-177, can uptake 1.5 wt % hydrogen under similar conditions [33]. The low hydrogen adsorption capacities in porous MOFs with high surface areas and large pore volumes are presumably due to weak interactions between hydrogen molecules and the frameworks [6].

Perhaps counterintuitively, smaller pores actually take up hydrogen more effectively than very large ones [16]. Reducing the pore size allows the H₂ molecule to interact with multiple portions of the framework; in a smaller pore, the attractive potential fields of opposite walls overlap [21]. This has been extensively explored as a strategy to increase hydrogen–framework interactions, thereby enhancing hydrogen uptake [6,20]. Systematic investigation of pore sizes on hydrogen uptake was recently exemplified in a series of NbO-type [34] and twisted borocite-type [35] porous MOFs based on tetracarboxylate and trigonal-planar tricarboxylate organic ligands, respectively. Extension of the organic ligands leads to a proportional increase in pore size but decrease in hydrogen uptake at 77 K/1 atm. These studies also indicate an ideal pore size of ~6 Å, which may allow the monolayer coverage of dihydrogen molecules with kinetic diameter of 2.89 Å on the opposites of pore walls, leading to optimal interaction between the H₂ molecules and the framework, thus maximizing the total van der Waals (vdW) forces acting on H₂ [21].

Employing short organic linkers is an effective way to achieve small pore sizes in porous MOFs, and an alternative strategy for reducing pore sizes can turn to interpenetration, which is the intergrowth of two or more identical frameworks and is usually favored by the use of longer linkers [36]. The typical effect of interpenetration on porosity is to subdivide large single pores, each bounded by the entire organic linker, into several smaller ones, each bounded by smaller portions of the organic linker [16]. The effects of catenation on hydrogen adsorption was illustrated by hydrogen adsorption studies on IRMOFs, which revealed that interpenetrating IRMOF-9, IRMOF-11, and IRMOF-13 showed higher hydrogen adsorption capacities than non-interpenetrating IRMOF-1, with the effect directly related to the reduction of pore diameter due to interpenetration formation [37]. The evaluation of interpenetra-

tion as an independent criterion on the hydrogen uptake of a porous MOF has recently been reported in the studies of interpenetrating PCN-6 and the non-interpenetrating counterpart PCN-6', revealing that interpenetration leads to 29 % increase in gravimetric hydrogen uptake at 77 K/1 atm [38]. The enhanced hydrogen uptake can be ascribed to the strengthened hydrogen–ligand interactions as a result of interpenetration as elucidated by INS studies [32].

Although organic linkers are not the primary adsorption sites for hydrogen, they can play an important secondary role in increasing adsorption further [16]. Increasing the aromaticity of the organic linker has been proved to be an effective way to enhance hydrogen adsorption capacity in porous MOFs [24,36,39]. A typical example is the recently reported NbO-type porous MOF PCN-14, which was built from an anthracene derivative, 5,5'-(9,10-anthracenediyl)di-isophthalate (Scheme 1c). PCN-14 exhibits a higher hydrogen adsorption capacity of 0.027 kg/kg at 77 K/1 atm than those based on tetracarboxylate organic ligands functionalized with C–C double bond or phenyl ring (Scheme 1) [40]. The improved hydrogen uptake in PCN-14 can be attributed to the more aromatic central anthracene ring.



Scheme 1 (a) *trans*-stilbene-3,3',5,5'-tetracarboxylate; (b) terphenyl-3,3',5,5'-tetracarboxylate; (c) 5,5'-(9,10-anthracenediyl)di-isophthalate.

One of the advantages in porous MOFs when compared to carbon materials is that metal ions incorporated in porous MOFs have much higher hydrogen-binding energies than carbon materials do, and the metal ions are the preferential adsorption sites for hydrogen as revealed by recent neutron studies [6,15,16]. The impregnation of coordinative UMCs, which are usually very reactive and are known to play an important role in catalysis, into porous MOFs is very attractive for hydrogen adsorption due to their significantly high hydrogen affinity [6,20,21,41,42]. An effective way to achieve coordinative unsaturation of the metal ions is to liberate the terminal bound labile solvent (aqua) ligands by thermal activation (usually 100–200 °C under vacuum), provided the porous framework integrity is retained after the process [6,16]. Chen et al. have shown that the removal of axial aqua ligands from Cu₂ paddle-wheel SBUs via thermal activation exposes the coordinatively unsaturated Cu centers in MOF-505, leading to a hydrogen uptake as high as 0.0247 kg/kg at 77 K/1 atm [43].

The contribution from UMCs to hydrogen adsorption capacity is quite remarkable, but sometimes the UMCs are misaligned in the porous MOF structures. Utilizing the “close-packing” strategy, Wang et al. constructed porous MOFs with polyhedral cage structures which allow the rational alignment of UMCs (Fig. 1). This facilitates the direct interaction between UMCs and hydrogen molecules within the void, resulting in by far the highest hydrogen uptake capacity of 0.0305 kg/kg at 77 K/1 atm in PCN-12 with aligned UMCs, which is 27 % higher than that of the misaligned PCN12' (0.024 kg/kg) [44].

Although extensive studies have been focused on hydrogen uptake at 77 K/1 atm, increasing attention is being drawn to high-pressure hydrogen studies because of their direct application in practical on-board hydrogen storage, as required by the DOE goals [2,6,15,16,21–23]. In high-pressure studies, two quantities, excess adsorption and absolute (or total) adsorption, are frequently used to describe hydrogen adsorption in porous MOFs. Excess adsorption can be directly accessible experimentally, and it is the amount of adsorbed gas interacting with the frameworks in the presence of the adsorbent. In contrast, absolute (or total) adsorption is the sum of excess adsorption, and the amount of gas would be

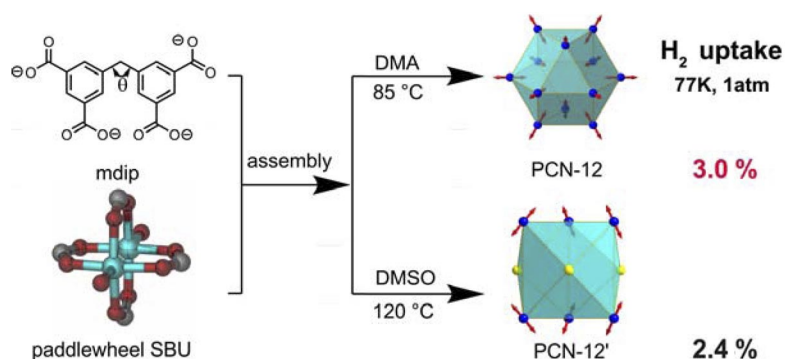


Fig. 1 Synthesis, open metal site alignment, and hydrogen uptake of the two MOF polymorphs: PCN-12 and PCN-12'. (Reprinted with permission from ref. [41], copyright © 2008, Wiley-VCH.)

found within the pore volume even in the absence of the adsorbent, which can be estimated using the crystal density of a porous MOF. From the viewpoint of hydrogen storage and delivery, the absolute (or total) amount is the more relevant quantity [45].

Current research of high-pressure hydrogen storage on porous MOFs has been focused on the liquid nitrogen temperature of 77 K, and existing studies have demonstrated that the hydrogen uptake capacities scale up with their surface areas [2,6,15,16,21–23]. Since a high surface area has been recognized as the first prerequisite for cryogenic hydrogen storage application of porous MOFs, extensive efforts have been devoted to the ligand design to achieve high surface areas [2]. Extension of the tricarboxylate, tetracarboxylate, and hexacarboxylate ligands as well as the combination of dicarboxylate and triarboxylate ligands [46] has recently been proved an effective strategy to accomplish high surface areas in porous MOFs (Fig. 2), and those high-surface-area porous MOFs indeed demonstrate exceptional hydrogen storage capacities [2,6]. Current records for hydrogen uptake in porous MOFs are held by NU-100, which has an extremely high excess adsorption capacity of 99.5 mg/g due to its Brunauer–Emmett–Teller (BET) surface area of 6143 m²/g [47], and MOF-210 which demonstrates an unprecedented absolute storage capacity of 167 mg/g benefiting from its exceptional Langmuir surface area of 10400 m²/g [14].

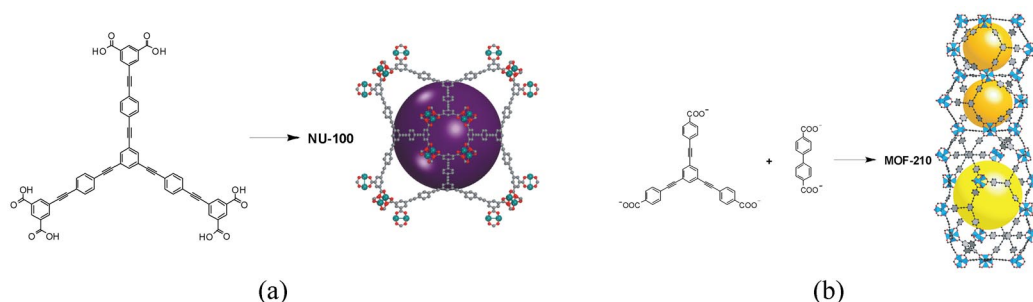


Fig. 2 (a) A hexatopic ligand utilized to construct NU-100; (b) combination of tritopic and ditopic ligands for the construction of MOF-210. (Reprinted with permissions from ref. [47], copyright © 2010, Macmillan and ref. [14], copyright © 2010, *Science*, AAAS.)

Although the cryogenic high-pressure hydrogen storage capacities of some porous MOFs can achieve or even surpass the DOE target values, their hydrogen uptake capacities at room temperature are still very low (less than 0.015 kg/kg) [2], which is due to their low hydrogen adsorption enthalpies

of just a few kJ/mol. To ensure high hydrogen uptake at ambient temperature, a desired binding energy of ca. 20 kJ/mol in the overall hydrogen-loading range has recently been proposed [48], and various strategies have been explored to increase the hydrogen adsorption enthalpy to approach this value [6,23]. The introduction of UMCs [41] and chemical doping with alkali metals [49] seem very attractive to enhance hydrogen adsorption enthalpies in porous MOFs; however, the high adsorption enthalpies can only be achieved at very low hydrogen coverage, and their abrupt decline to 5–6 kJ/mol with the increase of hydrogen loadings results in almost negligible improvement of hydrogen uptakes at room temperature under high pressure [2,6,15,16]. To obtain high hydrogen adsorption enthalpies in the overall range of hydrogen coverage, an intriguing method of secondary hydrogen spillover has recently been developed by Yang et al. This method not only significantly enhances the average hydrogen adsorption enthalpies to ~20 kJ/mol, but also remarkably improves the hydrogen uptake capacity up to 0.03–0.04 kg/kg in porous MOFs at 298 K and 10 MPa [50]. Nevertheless, difficulties in reproducing some of the experimental results as well as the cost of expensive Pt cast a shadow on the outlook of such a fascinating technique. Exploration of porous MOFs with high hydrogen uptake at ambient temperature for practical on-board storage applications still has a long way to go [2,6].

Methane storage in porous MOFs

Methane, the primary component of natural gas, is also considered an ideal energy gas. As with hydrogen, it suffers the lack of effective storage for mobile application [2,6,16]. The DOE target for methane storage has been set at 180 v(STP)/v (STP equivalent of methane per volume of adsorbent material storage system) under 35 bar and near-ambient temperature, which is based on the energy density of adsorbed natural gas comparable to that of current compressed natural gas technology [51].

Although the first reported methane sorption study using porous MOFs could date back to as early as 1997 [52], the field of methane storage on MOFs has not expanded as fast as the hydrogen storage field, and reports on methane storage in porous MOFs are much less than hydrogen [2,6,16].

Like cryogenic high-pressure hydrogen storage, the high-pressure gravimetric methane uptake of porous MOFs at room temperature scales up with the surface areas, and exceptionally high gravimetric methane adsorption capacities have been observed in some high-surface-area porous MOFs [2,14]. However, different from hydrogen storage, the methane storage target set by DOE is only for volumetric capacity in the unit of v(STP)/v. In most cases, the low density of a high-surface-area porous MOF decreases the volumetric methane uptake despite its high gravimetric uptake value [53]. This then requires a compromise between the surface area and the crystal density, which could be predicted via theoretical calculations [2,6,15].

Inspired by a recent theoretical simulation [54], a high excess methane uptake capacity of 220 v(STP)/v [absolute: 230 v(STP)/v] at 290 K and 35 bar has been achieved in the porous MOF PCN-14, which is constructed from 5,5'-(9,10-anthracenediyl)-diisophthalate ligand (Scheme 1) and Cu₂ paddlewheel motif [55]. This represents the first case exceeding the DOE methane storage target for porous MOFs, despite the fact that the capacity was calculated based on its crystallographic density instead of the real packing density. The unprecedentedly high methane uptake capacity of PCN-14 can be attributed to the existence of nanoscopic cages enclosed by the anthracene-derivative ligands, which strengthen the methane–framework interactions as evidenced by the exceptional methane adsorption enthalpies of ~30 kJ/mol at low methane coverage.

In addition to ligand functionalization, the exposure of open metal sites has been proved to be another effective way to achieve high methane uptake in porous MOFs [2,6]. A high methane adsorption capacity of 190 v(STP)/v [absolute: 200 v(STP)/v] at 298 K and 35 bar has been observed in the porous MOF Ni₂(dhtp) (dhtp = 2,5-dihydroxyterephthalate) after thermal activation to expose the open Ni sites [56].

The contribution of open metal sites to methane uptake has been elucidated by neutron powder diffraction studies of CD_4 adsorption in HKUST-1, PCN-11 [57], and a series of isomorphous porous MOFs with different UMCs [56], revealing that open metal sites serve as the primary methane adsorption sites. Neutron powder diffraction studies of CD_4 adsorption in HKUST-1 and PCN-11 have also identified the vdW potential pocket sites residing in the small cages and at their windows as the secondary strong adsorption sites for methane molecules (Fig. 3) [57]. The specific methane adsorption sites in porous MOFs have been further confirmed by single-crystal structure analysis of methane-adsorbed $\text{Zn}_2(\text{bdc})_2(\text{dabco})$ utilizing synchrotron radiation. These kinds of mechanistic studies provide very useful information for future design of porous MOFs with high methane storage capacities for practical usage [58].

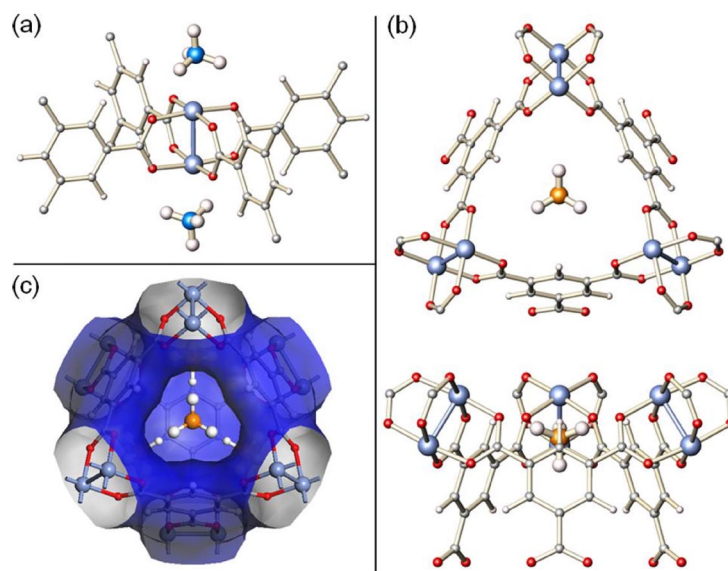


Fig. 3 (a) Experimentally determined partial structure of the HKUST-1 crystal with CD_4 molecules adsorbed at (a) the open Cu sites and (b) the small cage window sites (top and side views). (c) vdW surface of the small octahedral cage in HKUST-1 (derived by using N_2 as probe molecules), showing the size and geometry of the pore window in an excellent match with a methane molecule. (Reprinted with permission from ref. [57], copyright © 2010, Wiley-VCH.)

Acetylene storage in porous MOFs

Acetylene gas is another important energy gas and is the starting material for various chemical fine products and electric materials [59]. However, the highly explosive nature of acetylene in the absence of oxygen even at room temperature limits its safe storage pressure below 0.2 MPa [60], and this prompts the search for novel materials with high acetylene storage capacity at ambient temperature and low pressure [61]. Benefiting from their functionalizable nanospace [5], porous MOFs have recently been screened for acetylene storage.

Initial studies of acetylene storage in porous MOFs were dedicated to constricting the pore sizes to increase acetylene–framework interactions [62]. This was proved an effective way to enhance the acetylene adsorption enthalpies; however, the low surface areas of the porous MOFs with small pore sizes have largely limited their acetylene uptake capacities.

Systematic investigation of the impacts of ligand functionalization on acetylene uptake was performed on a series of isorecticular pillared porous MOFs based on the dicarboxylate ligands functional-

ized with phenyl ring, naphthalene ring, or anthracene ring [63]. The studies indicated that the porous MOFs constructed from 1,4-naphthalenedicarboxylate and 9,10-anthracenedicarboxylate demonstrated high acetylene uptake capacities of over $100 \text{ cm}^3/\text{g}$ at 298 K/1atm, which are significantly higher than other conventional porous materials. The excellent observed acetylene performances can be ascribed to the remarkable interactions between the acetylene gas molecules and the fused aromatic rings.

The exposure of open metal sites has been proved to be an effective method to increase hydrogen and methane uptake in porous MOFs, and this strategy has also recently been employed by Chen et al. to successfully improve acetylene adsorption capacities in porous MOFs [64]. Thermally liberating the axial aqua ligands on the Cu paddlewheel motifs lead to a high acetylene uptake capacity of $177 \text{ cm}^3/\text{cm}^3$ ($201 \text{ cm}^3/\text{g}$) at 295 K/1 atm in HKUST-1, and an even higher volumetric storage capacity of $230 \text{ cm}^3/\text{cm}^3$ together with the exceptional acetylene adsorption enthalpy of 50.1 kJ/mol at the low coverage was achieved in $\text{Co}_2(\text{dhtp})$ after exposure of the open Co metal sites [65].

As with hydrogen and methane adsorption, neutron powder diffraction has also been employed to study the mechanism of acetylene adsorption in porous MOFs. Neutron powder diffraction studies of C_2D_2 in HKUST-1 [64] and $\text{Co}_2(\text{dhtp})$ [65] (Fig. 4) have identified the specific adsorption sites for acetylene molecules, and revealed open metal centers as the primary strong binding sites similar to what is observed for hydrogen and methane adsorption in porous MOFs, further highlighting the important role of open metal sites for energy gas storage in porous MOFs.

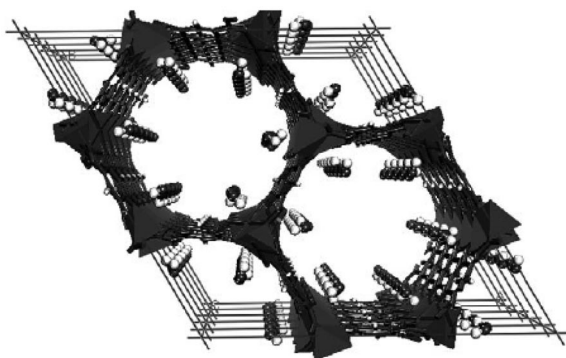


Fig. 4 Crystal structure of $[\text{Co}_2(\text{dhtp})]$ with loading of 0.54 C_2D_2 per Co viewed along the c axis, exhibiting the high density of adsorbed acetylene molecules in pseudo-1D arrays. (Reprinted with permission from ref. [65], copyright © 2010, Wiley-VCH.)

CO₂ CAPTURE APPLICATION OF POROUS MOFs

The widespread concern for the prospect of a worsening climatic situation due to global warming has drawn unprecedented public attention to the issue of CO_2 emission [2]. The annual global emissions of CO_2 have escalated by about 80 % in the past 40 years, and this dramatic rise has been ascribed to the rapid expansion of the energy consumption worldwide with an increasing dependence on the combustion of fossil fuels (coal, petroleum, and natural gas), which contribute 86 % of the anthropogenic greenhouse gas emission [66]. To stabilize the level of atmospheric CO_2 , it is urgent to develop viable CO_2 capture and sequestration technologies [2]. Current technologies are dictated by amine-based wet-scrubbing systems, which, however, suffer the drawbacks of considerable energy requirements for solvent regeneration and necessary use of inhibitors to control corrosion and oxidative degradation [67]. In contrast, adsorption of CO_2 using highly porous solid materials possesses the advantage of energy efficiency and facile regeneration, and it has been of increasing interest for CO_2 capture applications [68,69]. Bearing the features of high surface areas and functionalizable pore walls, porous MOFs have

in recent years attracted great attention for CO₂ capture applications particularly as physical adsorbents for CO₂ storage [2].

The high surface areas of porous MOFs can afford them with enhanced capacities for CO₂ capture at moderate pressures compared with zeolites and other porous materials [69]. This has been proven in the seminal work by Yaghi et al., revealing that MOF-177 with CO₂ uptake capacity of 33.5 mmol/g (350 cm³/cm³) at 298 K/32 bar benefiting from its high Langmuir surface area of 5640 m²/g, can surpass the benchmark materials zeolites 13X and activated carbon MAXSORB by a factor of over 1.5 in both gravimetric and volumetric capacities [70].

Existing studies have validated surface area as the primary factor influencing the CO₂ uptake capacities of porous MOFs, which scale up with the Langmuir surface areas [2,14,47,53,70]. The peak gravimetric uptake for CO₂ has been reported in porous MOFs with ultrahigh surface areas. The porous MOFs, MOF-200 and MOF-210, both of which have an exceptionally high Langmuir surface area of 10 400 m²/g, exhibit the highest capacity for CO₂, taking up to 2400 mg/g (54.5 mmol/g) at 50 bar [14]. Other high-surface-area porous MOFs such as NU-100 with a BET surface area of 6143 m²/g also possess a high CO₂ uptake capacity (2043 mg/g for NU-100) [46].

One advantage of porous MOFs lies in the ability to functionalize their pore walls with active groups such as amines by ligand design [71] or via postsynthetic modification approaches [11]. The later strategy has been exploited to increase CO₂ uptake as well as CO₂ binding energy in porous MOFs. Treated with NH₄F, a high CO₂ uptake capacity of 40 mmol/g (390 cm³/cm³) has been achieved in MIL-101 [72]. Modifying the bridging ligands with amine-based groups [73] or grafting alkylamine functionality onto a UMC has significantly enhanced CO₂ adsorption enthalpies of porous MOFs (Fig. 5) [74]. The enhanced CO₂ binding energies also improve the capability of preferential adsorption of CO₂ over other gases such as N₂, CH₄ in porous MOFs [75], which is another important criterion for CO₂ capture and will be discussed in the following section.

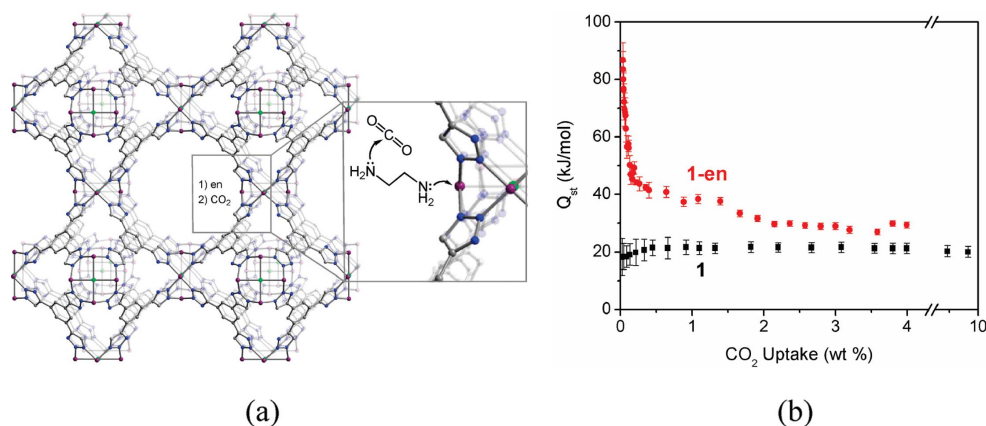


Fig. 5 (a) Portion of the framework HCu[(Cu₄Cl)₃(BTtri)₈(en)₅] showing one of the en-functionalized Cu²⁺ sites and its interaction with a CO₂ molecule; (b) isosteric heat of adsorption for CO₂ showing the en-functionalized framework (red) exhibiting enhanced Q_{st}. (Reproduced with permission from ref. [74], copyright © 2008 American Chemical Society.)

GAS SEPARATION APPLICATION OF POROUS MOFs

Gas separation and purification are of great importance in industry. Conventional gas separation methods rely heavily on cryogenic distillation, which is very energy-consuming and costly [6]. The introduction of membrane- and adsorption-based technologies has revolutionized gas separation in industry,

and they are more energy-efficient and environmentally friendly. In particular, adsorptive separation will likely play a critical role in future energy and environmental technologies [76,77]. Current adsorbents used for gas separation in industry are dominated by inorganic zeolites and porous carbon materials; however, new adsorbents are still needed to optimize the separation processes to make them commercially more attractive [6,15,77]. Featuring design amenability, tunable pore size, and functionalizable pore walls, porous MOFs known as a new type of zeolite analogues have great potential in gas separation applications [6]. A complete review of gas separation in porous MOFs can be found in ref. [77]; in order to avoid repetition, herein, we will just highlight some representative work reported in recent years.

Molecular-sieving effect in porous MOFs

The molecular-sieving effect has been frequently observed in inorganic zeolites [76], and it is mainly based on size-exclusion, which means molecules with size smaller than the pore size can pass through while larger ones are excluded [6,15]. This ascribes to the primary principle for most selective gas adsorption processes in porous materials with uniform micropores [6,77].

Controlling the pore size of an adsorbent is essential for effective gas separation [77]. To this point, the amenability to design renders the possibility to rationally tune the apertures of porous MOFs to a certain size for selective adsorption of specific gas molecules [6].

One effective way to constrict pore sizes of porous MOFs for gas separation is by utilizing short bridging ligands [6,15]. This was exemplified in a recently reported microporous manganese formate MOF [78]. The utilization of the short formate ligand results in a very small aperture size, which can discriminate H_2 from N_2 , and CO_2 from CH_4 . Another good strategy to confine pore sizes is increasing the bulkiness of the struts, as recently illustrated in the microporous Zn MOF, PCN-13. PCN-13 is constructed from a bulky ligand 9,10-anthracenedicarboxylate (adc), and the bulkiness of the adc ligand constricts its pore size to $\sim 3.5 \times 3.5 \text{ \AA}$, which allows H_2 and O_2 to pass through the pores but excludes N_2 and CO [79].

Interpenetration has been well known as an effective way to reduce pore size of porous MOFs [36], and has been recently employed to confine the pore size for gas separation [6,15]. The introduction of triple interpenetration has afforded the capability to distinguish H_2 from N_2 and CO for the microporous MOF Zn(ADC) $(4,4'\text{-Bpe})_{0.5}$ [ADC = 4,4'-azobenzene dicarboxylate, 4,4'-Bpe = *trans*-bis(4-pyridyl)ethylene] [80]. Although the pore size resulting from double interpenetration is usually not tiny enough to selectively uptake small gas molecules, by shortening the pillared ligands via rational design, Chen et al. have successfully tuned the pore size of the doubly interpenetrated primitive cubic nets based on bidentate pillar linkers and bicarboxylates to $\sim 3.6 \text{ \AA}$, which exhibits selective adsorption of H_2 over Ar, N_2 , and CO [81]. Linking interpenetration with coordinative bonds has proved to be another good way to further confine the pore size of doubly interpenetrated porous MOFs for selective gas adsorption, as recently well demonstrated in the porous MOF, PCN-17 which possesses doubly interpenetrated frameworks coordinatively linked by the in situ generated sulfate ligands. The coordinatively linked interpenetration renders PCN-17 to selectively uptake H_2 and O_2 over N_2 and carbon monoxide as well as affords the high thermal stability of up to $480 \text{ }^\circ\text{C}$ while maintaining permanent porosity [82].

Mesh-adjustable molecular sieves

For inorganic zeolite molecular sieves and most rigid porous MOFs, their mesh sizes are usually fixed due to bond rigidity [76]. When the size disparity of two gases is very small, those rigid molecular sieves with fixed mesh sizes can hardly be discriminated from the gases. To this point, mesh-adjustable molecular sieves (MAMSs) that can always meet the separation needs are highly desirable, and they should be very useful for gas separations [6,15,77].

Although MAMSs are difficult to achieve in inorganic zeolites, the dynamic features of porous MOFs could afford them flexible pore sizes [83]. Based on the amphiphilic ligand 5-*tert*-butyl-1, 3-benzenedicarboxylate (BBDC), the first MOF-based mesh-adjustable molecular sieve, MAMS-1, was recently successfully constructed [84]. MAMS-1 has a trilayer structure and consists of hydrophilic channels and hydrophobic chambers, which are interconnected with each other through a pair of BBDC ligands serving as the adjustable gate at their interface. Simply varying the temperature, the mesh size of MAMS-1 can be tuned anywhere from 2.9 and 5.0 Å as estimated from the variable temperature gas adsorption studies between 77 and 298 K. Mechanistic studies suggest that the hydrophobic chambers are the site of gas storage, yet the gas must first pass through the fully activated hydrophilic channels to enter the hydrophobic chambers via gates of the BBDC ligands at the interface of hydrophilic channels and hydrophobic chambers. The gates of the BBDC ligands open almost linearly with increasing temperatures to gradually let gas molecules of certain sizes enter the hydrophobic gas storage chambers. The extension of BBDC ligand to the 4'-*tert*-butyl-biphenyl-3,5-dicarboxylate (BBPDC) ligand leads to a series of isostructural MAMSs (MAMS-2, MAMS-3, and MAMS-4, prepared with Zn, Cu, and Co metal ions, respectively) which display similar temperature-induced molecular-sieving effects to those observed in MAMS-1 [85]. For all of the four MAMSs, a linear relationship has been found between mesh size and temperature, $D = D_0 + \alpha T$ (D = mesh size at temperature T K, D_0 = mesh size at 0 K, and α -constant), D_0 and α are related to the functional organic group of *tert*-butyl (Fig. 6). By adjusting D_0 and α , which could be achieved by changing different functional organic groups, it is expected to lead to some new MAMSs which might be omnipotent for gas separation at near-ambient temperatures [6,15,77].

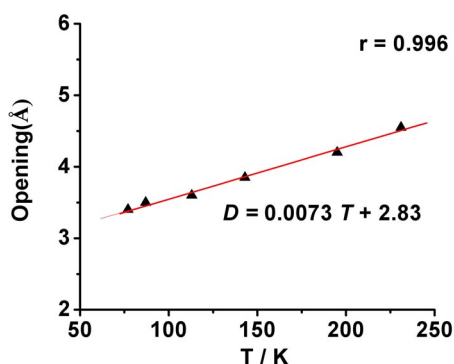


Fig. 6 Temperature and gate-opening relationship of MAMS-2. (Reproduced with permission from ref. [85], copyright © 2009 American Chemical Society.)

Kinetic separation in porous MOFs

Different from the size-exclusion-based molecular-sieving effect, kinetic separation is achieved by virtue of the differences in diffusion rates of different molecules due to different adsorbate–surface interactions [6,15,77].

Kinetic separation of mixed C_8 alkylaromatic compounds (*p*-xylene, *o*-xylene, *m*-xylene, and ethylbenzene), which is one of the most challenging separations in chemical industry due to the similarity of their boiling points [86], was investigated using three porous MOFs: HKUST-1, MIL-53, and MIL-47 in the liquid phase. Chromatographic experiments indicated that MIL-47 stands out from the three investigated porous MOFs in terms of uptake capacity and high selectivity, promising its potential for future practical application in industry [87].

The kinetic separation of hexane isomers, which represents a very important process in the petroleum industry [88] was also studied using a 3D microporous MOF, $\text{Zn}(\text{BDC})(\text{Dabco})_{0.5}$ by fixed-bed adsorption. Benefitting from its narrow channels of $3.8 \times 4.7 \text{ \AA}$, which can exclusively take up linear nHEX while blocking branched hexane isomers, it exhibited extraordinary separation selectivity to separate branched hexane isomers from linear nHEX, which affords the promise for its applications in the very important industrial process of hexane-isomers separation [89].

Due to the very close relative volatilities and molecular sizes of propane/propylene, their separation represents another very difficult process in the chemical industry. A promising solution for this issue has recently been demonstrated in a series of Zn-based imidazolate zeolitic frameworks, which exhibit impressive capability for kinetic separation of propane and propylene [90]. This also distinguishes porous MOFs from other porous materials for potential practical application in propane–propylene separation.

Porous MOFs for chromatographic application

The good performances of porous MOFs on kinetic separations afford them great opportunities for chromatographic application [77]. Packing the column of gas chromatography (GC) with a microporous MOF (MOF-508), Chen et al. demonstrated for the first time the utilization of porous MOFs for GC separation of alkanes. MOF-508 contains 1D pores of $\sim 4.0 \times 4.0 \text{ \AA}$, which can selectively accommodate linear alkanes and discriminate branched alkanes (Fig. 7). The subtle matching of the size and shape of the alkanes with the micropores of MOF-508 leads to different vdW interactions, thus resulting in selective GC separation of alkanes in the MOF-508 column [91].

The high-resolution GC separation of xylene isomers and ethylbenzene using porous MOFs has recently been illustrated by Pan et al. [92]. Taking advantage of the coordinatively unsaturated sites and large pore volume of MIL-101, they fabricated the MIL-101 coated capillary column with a dynamic coating method, which leads to good performance of high-resolution GC separation of xylene isomers and ethylbenzene. More recently, they also successfully demonstrated the utilization of ZIF-8, which contains hydrophobic micropores as the stationary phase for high-resolution GC separation of linear alkanes [93].

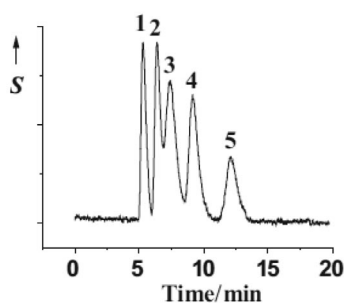


Fig. 7 MOF-508 packed column for GC separation of an alkane mixture containing 2-methylbutane (1), *n*-pentane (2), 2,2-dimethylbutane (3), 2-methylpentane (4), and *n*-hexane (5). S = thermal conductivity detector response. (Reprinted with permission from ref. [91], copyright © 2006, Wiley-VCH.)

The evaluation of porous MOFs for liquid chromatographic separations has been performed as well. With HKUST-1 or MOF-5 as the stationary phase, excellent separation of organic compounds including benzene, ethylbenzene, styrene, naphthalene, anthracene, phenanthrene, pyrene, 1,3,5-triphenylbenzene, and 1,3,5-tris(4-bromophenyl)benzene was achieved due to a combination of molecular-sieving and adsorption effects [94].

The exciting results from existing studies greatly promise porous MOFs as a new type of stationary-phase material for chromatographic applications.

Porous MOFs for membrane application

Membrane-based gas separations are very useful in industry, and zeolite membranes have been well developed [76]. As a new type of zeolitic analogues, porous MOFs hold great potential as a new type of membrane materials [77]. However, the difficulty for porous MOFs in membrane application lies in how to prepare a continuous crack-free membrane without leaks [95]. Using a “twin copper source” technique, Zhu et al. successfully prepared the $\text{Cu}_3(\text{btc})_2$ MOF membrane supported on a Cu net (Fig. 8) [96]. The oxidized Cu net provides homogeneous nucleation sites for the continuous crystal membrane growth in the solution, which contains Cu^{2+} ions and organic ligand H_3btc . The investigation of membrane-based separation of H_2/N_2 , H_2/CO_2 , and H_2/CH_4 mixtures demonstrated that the prepared porous MOF membrane has a high H_2 permeation flux of $0.107 \text{ mol m}^{-2} \text{ s}^{-1}$, and an excellent permeation selectivity for H_2 with the separation factor being 7.04, 6.84, and 5.92, respectively (298 K, 1 atm with a 1:1 volume ratio gas mixture). The permeability and selectivity of this porous MOF-based membrane surpass those of conventional zeolite membranes. In addition, its good stability and recyclability promise great potential for practical applications in separation or purification of H_2 .

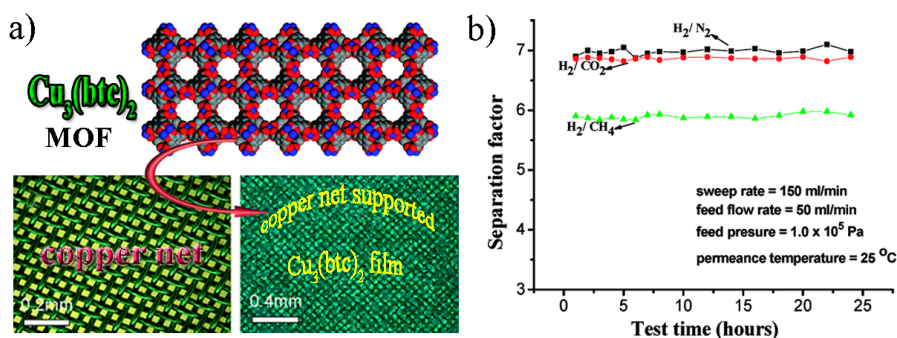


Fig. 8 (a) Structure of $\text{Cu}_3(\text{btc})_2$ porous MOF and optic micrographs of the Cu net and Cu net-supported $\text{Cu}_3(\text{btc})_2$ membrane. (b) Plot of H_2/N_2 , H_2/CH_4 , and H_2/CO_2 separation factor of the Cu net-supported $\text{Cu}_3(\text{btc})_2$ membrane with change in test time. (Reproduced with permission from ref. [77], copyright © 2009, The Royal Society of Chemistry.)

CATALYSIS APPLICATION OF POROUS MOFs

Catalysis represents another promising application for porous MOFs and has attracted escalating interests in recent years. Since a few authoritative review articles in this aspect have appeared [97–99], herein, we will only briefly emulate some major types of catalyst systems utilized in porous MOFs.

Porous MOFs as catalyst host matrices

Using inorganic porous materials as catalysts support or host has been well developed in the field of heterogeneous catalysis [99]. The nanospace of porous MOFs not only can provide the ideal room to store gas molecules, but also can accommodate catalytically active nanoparticles or guest molecules, making them good catalyst host matrices [97].

The introduction of metal nanoparticles into porous MOFs may allow their uniform dispersion with maximum exposure of active sites. Utilizing chemical vapor deposition with organometallic com-

plexes as precursors followed by reduction, Fischer et al. successfully introduced metallic Cu and Pd nanoparticles into MOF-5, and the resulting solids demonstrated good activities for methanol synthesis (Cu@MOF-5) and hydrogenation of cyclooctene, respectively [100]. The impregnation of Pd nanoparticles into activated MIL-101 via a solution process leads to high activities for the water-mediated Suzuki–Miyaura and Ullmann coupling reactions of aryl chlorides, which benefits from the highly dispersed Pd nanoparticle supported on MIL-101 as evidenced from transmission electron microscopy (TEM) studies [101].

The incorporation of metalloporphyrins, which are widely used for homogeneous catalysis, into porous MOFs has recently been demonstrated by Eddaoudi et al. (Fig. 9) [102]. With the rho-ZMOF as host matrices, the encapsulated free-base porphyrin can be metallated with Mn, Co, Zn, or Cu ions, and the Mn version demonstrated good performance on the oxidation of cyclohexane to cyclohexanol and cyclohexanone using *tert*-butyl hydroperoxide (TPHP) oxidant.

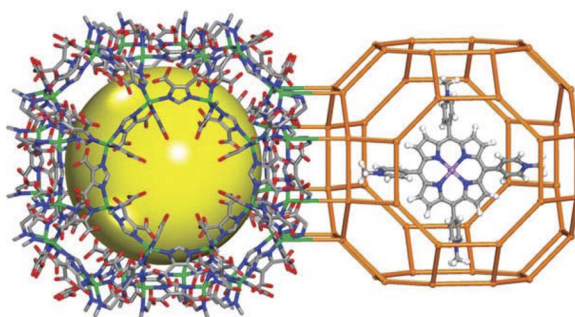


Fig. 9 Pore structure of rho-ZMOF (left), and encapsulated $[H_2TMPyP]^{4+}$ porphyrin in rho-ZMOF a-cage (right). (Reproduced with permission from ref. [102], copyright © 2008 American Chemical Society.)

Catalysis in porous MOFs with open metal sites

The introduction of open metal sites into porous MOFs can offer a promising tool in catalysis because a regular arrangement of open metal sites on the channel walls could induce regio-, shape-, or size selectivity toward substrates or reaction intermediates [83,97,99].

An effective way to achieve open metal sites is utilizing thermal activation to liberate one or two labile solvent ligands coordinated to the metal sites, as widely employed to enhance hydrogen uptake capacity in porous MOFs [6,41]. The exposed open metal sites can serve as Lewis acid sites for catalysis reactions. Removing the coordinated water molecules to expose the open Cu(II) sites in HKUST-1, Kaskel and co-workers showed that HKUST-1 can function as a Lewis acid catalyst capable of catalyzing the cyanosilylation of benzaldehyde or acetone [103]. As recently demonstrated by Long et al., the exposure of two types of open Mn(II) sites in the porous MOF $Mn_3[(Mn_4Cl)_3BTT_8(CH_3OH)_{10}]_2$ [$H_3BTT = 1,3,5$ -benzenetris(tetrazol-5-yl)] results in not only high activity for cyanosilylation of aromatic aldehydes, but also good capability of catalyzing the Mukiyama aldol reactions which generally requires stronger Lewis acids than do cyanosilylations (Fig. 10) [104].

Another way to introduce open metal sites is directly using a metalloligand as the strut, and the metalloligand itself can serve as the catalytically active sites. This has been well demonstrated by Hupp and co-workers in the studies of acyl transfer reactions between *N*-acetylimidazole (NAI) and various pyridylcarbinols by utilizing porous MOFs based on a Zn(II)porphyrin strut [105].

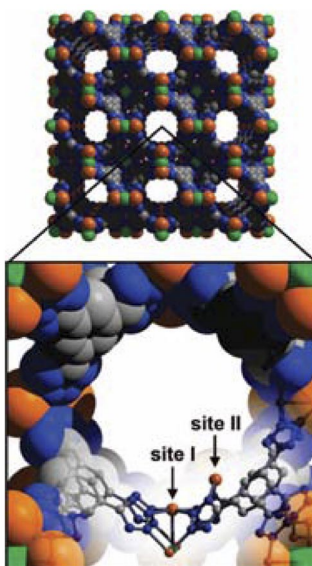


Fig. 10 Structure of the porous MOF, $\text{Mn}_3[(\text{Mn}_4\text{Cl})_3\text{BTT}_8(\text{CH}_3\text{OH})_{10}]_2$ showing the two types of exposed Mn^{2+} sites. (Reproduced with permission from ref. [104], copyright © 2008 American Chemical Society.)

Postsynthetic modification to graft catalytic sites onto porous MOFs

Postsynthetic modification is a useful tool to graft functionalities onto porous materials [11], and recently it has also been utilized to implant catalytic sites into porous MOFs. Modifying MIL-53(Al)- NH_2 with different anhydrides, Cohen et al. demonstrated that the maleic acid functionalized MIL-53(Al)-AMMal can act as a Brønsted acid catalyst and facilitate the methanolysis of several small epoxides [106].

Grafting the coordinatively unsaturated Cr(III) sites of MIL-101 with amines which react with chloropalladic acid followed by reduction with NaBH_4 , Chang and co-workers successfully trapped the Pd nanoparticles within the mesoporous cages, as confirmed by electron microscopy. The catalytic properties, validated on the Knoevenagel and Heck reactions, are drastically enhanced compared to those of the as-synthesized material (Fig. 11) [107].

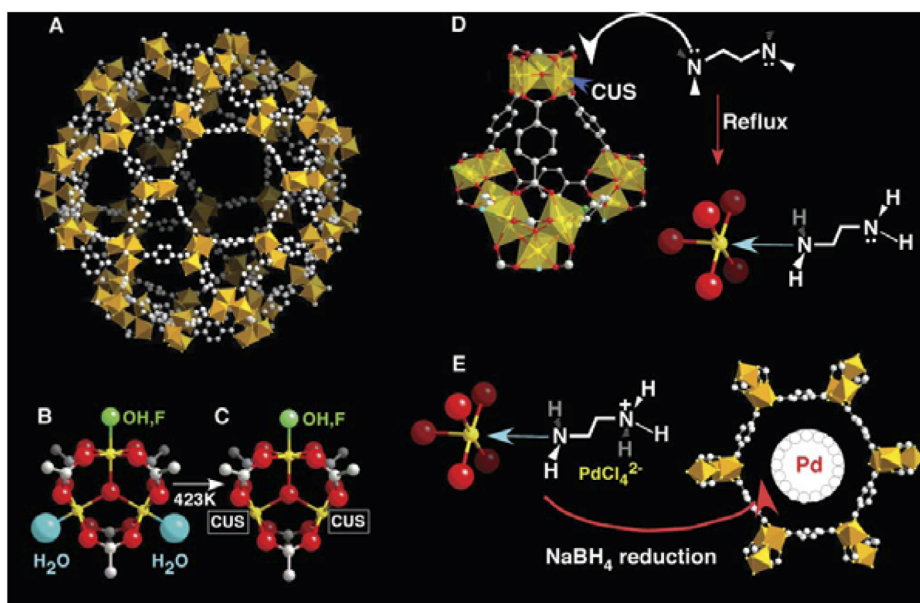


Fig. 11 Scheme of postsynthetic modification approach to generate catalytic metallic Pd nanoparticles in MIL-101. (Reprinted with permission from ref. [107], copyright © 2008, Wiley-VCH.)

Chiral catalysis in porous MOFs

One of the advantages for porous MOFs compared to inorganic zeolites lies in the possibility to exert homochirality either by direct utilization of homochiral ligands or via postsynthetic modification with chiral functionalities, and this offers them great promise for applications in chiral separation and chiral catalysis [98].

Using an enantiopure pyridine-functionalized derivative of tartaric acid, Seo et al. reported the synthesis of a homochiral metal–organic porous material, $[\text{Zn}_3(\mu_3\text{-O})(\text{L})_6] \cdot 2\text{H}_2\text{O} \cdot 12\text{H}_2\text{O}$ (POST-1, L = D-tartaric acid). (Fig. 12) [108]. The presence of the noncoordinated pyridyl groups is found to catalyze transesterification reactions, and the absence of significant catalysis when bulkier alcohols such as isobutanol, neopentanol, and 3,3,3-triphenyl-1-propanol are employed strongly suggests that the catalysis occurs within the channels of the porous MOF.

Employing a chiral salen(Mn) ligand of a pyridine-derivatized version of the well-known Katsuki–Jacobsen epoxidation catalysts as the strut, Hupp et al. built a two-fold interpenetrating pillared paddlewheel porous MOF and evaluated it as an asymmetric catalyst for olefin epoxidation reactions [109]. Their results reveal that heterogenization substantially increases the activity of the catalyst, yielding enantiomeric excesses that rival those of the free molecular analogue.

Instead of using homochiral ligands, Kim and co-workers developed an alternative strategy to render homochirality into the porous MOFs. With a chiral ligand as auxiliary, homochirality was successfully grafted in the porous MOF, $[\text{Zn}_2(\text{bdc})(1\text{-lac})(\text{dmf})] \cdot (\text{DMF})$. The produced homochiral porous MOF possesses permanent porosity as well as demonstrates remarkable catalytic activity with size and chemoselectivity, and high conversion in the oxidation of thioethers to sulfoxides [110].

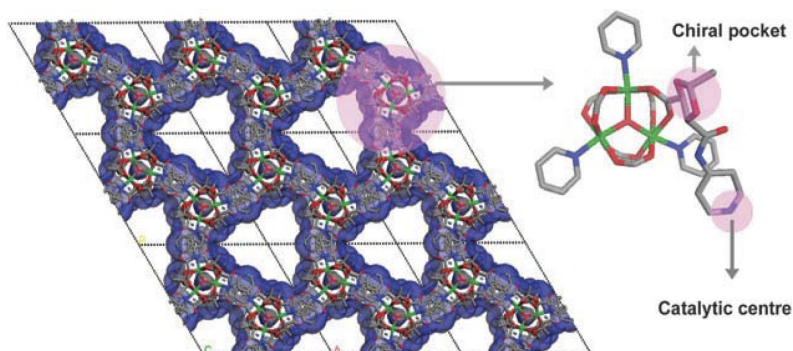


Fig. 12 1D equilateral triangular-shaped channel along the *c* axis of POST-1, with a size of 13.4 Å (left); coordination environment of metal centers of 8, showing the catalytic center and the chiral pocket (right). (Reproduced with permission from ref. [77], copyright © 2009, The Royal Society of Chemistry.)

FUEL CELL APPLICATION OF POROUS MOFs

One important component of proton exchange membrane fuel cell (PEMFC) is a protonically conducting but electronically insulating membrane placed between the anode and cathode, and the development of new types of proton-conductive materials is highly desirable due to some drawbacks of currently used Nafion membrane materials [111]. Bearing the advantage of a highly ordered structure as well as the controllable hydrophilicity and acidity of their frameworks via rational design of the frameworks, porous MOFs have recently been evaluated as a new type of proton conductor materials.

By encapsulating the proton-carrier molecule—imidazole in the 1D channels of two Al porous MOFs—Kitagawa et al. demonstrated that both of the two porous MOFs exhibit significant enhancement of proton conductivity at a temperature higher than 100 °C under anhydrous conditions, albeit their low proton conductivity at room temperature. The different proton conductivities of the two porous MOFs can be attributed to their different guest–host interactions [112].

Mimicking Nafion in which sulfonate groups play the key role on proton transport, Shimizu and co-workers implanted the sulfonate groups into the regular 1D pores of the porous MOF Na₃(2,4,6-trihydroxy-1,3,5-benzenetrisulfonate) (named β-PCMOF2) (Fig. 13a), which exhibits impressive proton conductivity [113]. Modulating β-PCMOF2 with the controlled loading of 1H-1,2,4-triazole (Tz) guests within the pores, a high proton conduction of 5×10^{-4} S cm⁻¹ at 150 °C in anhydrous H₂ was reached (Fig. 13b). The potential of β-PCMOF2 as a gas separator membrane was also confirmed by incorporating the partially loaded MOF (β-PCMOF₂(Tz)_{0.45}) into a H₂/air membrane electrode assembly, which gave an open-circuit voltage of 1.18 V at 100 °C, proving the resulting membrane to be gas tight.

By introducing NH₄⁺ ions using the anionic framework [Zn₂(ox)₃]₂^{-∞} (ox = oxalate) and putting carboxyl end groups of adipic acid in its honeycomb-shaped void, Sadakiyo et al. demonstrated that the porous MOF (NH₄)₂(adp)-[Zn₂(ox)₃]₂·3H₂O showed a superprotonic conductivity of 10⁻² S cm⁻¹ at ambient temperature under 98 % RH conditions [114]. This value is comparable to that of Nafion currently used in PEMFC, and promises porous MOFs as a new type of proton conductive materials for practical use in fuel cells.

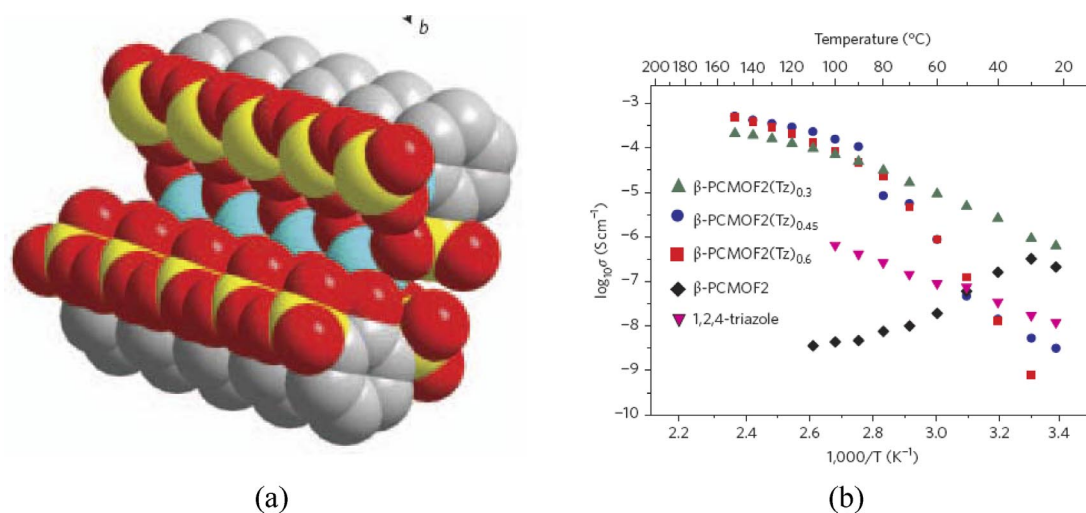


Fig. 13 (a) Space-filling diagram of the cross-section of one pore in β -PCMOF2, showing the high degree of sulfonation; (b) comparison of the Arrhenius plots of β -PCMOF2, [β -PCMOF2(Tz)_{0.3}], [β -PCMOF2(Tz)_{0.45}], and [β -PCMOF2(Tz)_{0.6}] measured in anhydrous H₂ atmospheres, σ , conductivity. (Reprinted with permission from ref. [113], copyright © 2009, Macmillan.)

CONCLUSIONS

As a new class of functional materials, porous MOFs have exhibited great potential for energy-related applications, ranging from gas storage to catalysis and from gas separation to fuel cell. Having witnessed such a great progress in the past decade, porous MOFs will continue to attract interest and inquiry by both academia and industry. The unique ability to engineer and decorate the nanospace inside their frameworks allows researchers to exert specific functionalities for targeted applications. In particular, with energy being one of the central issues for human beings, the needs for effective and efficient energy technologies will continue to increase, and porous MOFs are well positioned to remain at the forefront of this research.

ACKNOWLEDGMENTS

We would first like to thank IUPAC for giving us the precious opportunity to present this work to the special topic of Perspectives and Challenges for the International Year of Chemistry. We would also like to acknowledge the University of South Florida for financial support of this work.

REFERENCES

1. <www.doe.gov>
2. S. Ma, H.-C. Zhou. *Chem. Commun.* **46**, 44 (2010).
3. B. Chen, S. Xiang, G. Qian. *Acc. Chem. Res.* **43**, 1115 (2010).
4. M. E. Davis. *Nature* **417**, 813 (2002).
5. J. R. Long, O. M. Yaghi. *Chem. Soc. Rev.* **38**, 1213 (2009).
6. S. Ma. *Pure Appl. Chem.* **81**, 2235 (2009).
7. R. J. Kuppler, D. J. Timmons, Q.-R. Fang, J.-R. Li, T. A. Makal, M. D. Young, D. Yuan, D. Zhao, W. Zhuang, H.-C. Zhou. *Coord. Chem. Rev.* **253**, 3042 (2009).

8. D. J. Tranchemontagne, J. L. Mendoza-Cortes, M. O’Keeffe, O. M. Yaghi. *Chem. Soc. Rev.* **38**, 1257 (2009).
9. M. Eddaoudi, J. Kim, N. Rosi, D. Vodak, J. Wachter, M. O’Keeffe, O. M. Yaghi. *Science* **295**, 469 (2002).
10. M. O’Keeffe. *Chem. Soc. Rev.* **38**, 1215 (2009).
11. Z. Wang, S. M. Cohen. *Chem. Soc. Rev.* **38**, 1315 (2009).
12. H. K. Chae, D. Y. Siberio-Perez, J. Kim, Y. Go, M. Eddaoudi, A. J. Matzger, M. O’Keeffe, O. M. Yaghi. *Nature* **427**, 523 (2004).
13. G. Férey, C. Mellot-Draznieks, C. Serre, F. Millange, J. Dutour, S. Surble, I. Margiolaki. *Science* **309**, 2040 (2005).
14. H. Furukawa, N. Ko, Y. B. Go, N. Aratani, S. B. Choi, E. Choi, A. O. Yazaydin, R. Q. Snurr, M. O’Keeffe, J. Kim, O. M. Yaghi. *Science* **329**, 424 (2010).
15. S. Ma, C. D. Collier, H.-C. Zhou. “Design and construction of metal-organic frameworks for hydrogen storage and selective gas adsorption”, in *Design and Construction of Coordination Polymers*, M. Hong (Ed.), Chap. 12, p. 353, John Wiley, New York (2009).
16. D. J. Collins, S. Ma, H.-C. Zhou. “Hydrogen and methane storage in MOFs”, in *Metal-Organic Frameworks: Design and Application*, L. MacGillivray (Ed.), Chap. 8, p. 249, John Wiley, New York (2010).
17. DOE Office of Energy Efficiency and Renewable Energy Hydrogen, Fuel Cells & Infrastructure Technologies Program Multi-Year Research, Development and Demonstration Plan, available at: <<http://www.eere.energy.gov/hydrogenandfuelcells/mypp>>.
18. U.S. Department of Energy. Targets for on-board hydrogen storage systems: Current R&D focus is on 2015 targets with potential to meet ultimate targets (<http://www1.eere.energy.gov/hydrogenandfuelcells/storage/current_technology.html>).
19. N. L. Rosi, J. Eckert, M. Eddaoudi, D. T. Vodak, J. Kim, M. O’Keefe, O. M. Yaghi. *Science* **300**, 1127 (2003).
20. J. L. C. Rowsell, O. M. Yaghi. *Angew. Chem., Int. Ed.* **44**, 4670 (2005).
21. D. J. Collins, H.-C. Zhou. *J. Mater. Chem.* **17**, 3154 (2007).
22. D. Zhao, D. Yuan, H.-C. Zhou. *Energy Environ. Sci.* **1**, 222 (2008).
23. L. J. Murray, M. Dinca, J. R. Long. *Chem. Soc. Rev.* **38**, 1294 (2009).
24. S. S. Han, J. L. Mendoza-Cortes, W. A. Goddard III. *Chem. Soc. Rev.* **38**, 1460 (2009).
25. T. Yildirim, M. R. Hartman. *Phys. Rev. Lett.* **95**, 215504 (2005).
26. M. Dincă, A. Dailly, Y. Liu, C. M. Brown, D. A. Neumann, J. R. Long. *J. Am. Chem. Soc.* **128**, 16876 (2006).
27. V. K. Peterson, Y. Liu, C. M. Brown, C. J. Kepert. *J. Am. Chem. Soc.* **128**, 15578 (2006).
28. M. Dincă, W. S. Han, Y. Liu, A. Dailly, C. M. Brown, J. R. Long. *Angew. Chem., Int. Ed.* **46**, 1419 (2007).
29. J. L. C. Rowsell, J. Eckert, O. M. Yaghi. *J. Am. Chem. Soc.* **127**, 14904 (2005).
30. P. M. Forster, J. Eckert, B. D. Heiken, J. B. Parise, J. W. Yoon, S. H. Jung, J. S. Chang, A. K. Cheetham. *J. Am. Chem. Soc.* **128**, 16846 (2006).
31. Y. Liu, C. M. Brown, D. A. Neumann, V. K. Peterson, C. J. Kepert. *J. Alloys Compd.* **446–447**, 385 (2007).
32. S. Ma, J. Eckert, P. M. Forster, J. W. Yoon, Y. K. Hwang, J.-S. Chang, C. D. Collier, J. B. Parise, H.-C. Zhou. *J. Am. Chem. Soc.* **130**, 15896 (2008).
33. J. L. C. Rowsell, A. R. Millward, K. S. Park, O. M. Yaghi. *J. Am. Chem. Soc.* **126**, 5666 (2004).
34. X. Lin, J. Jia, X. Zhao, K. M. Thomas, A. J. Blake, G. S. Walker, N. R. Champness, P. Hubberstey, M. Schröder. *Angew. Chem., Int. Ed.* **45**, 7358 (2006).
35. X.-S. Wang, S. Ma, D. Yuan, J. W. Yoon, Y. K. Hwang, J.-S. Chang, X. Wang, M. R. Jørgensen, Y.-S. Chen, H.-C. Zhou. *Inorg. Chem.* **48**, 7519 (2009).
36. S. R. Batten, R. Robson. *Angew. Chem., Int. Ed.* **37**, 1460 (1998).

37. J. L. C. Rowsell, O. M. Yaghi. *J. Am. Chem. Soc.* **128**, 1304 (2006).
38. S. Ma, D. Sun, M. Ambrogio, J. A. Fillinger, S. Parkin, H.-C. Zhou. *J. Am. Chem. Soc.* **129**, 1858 (2007).
39. S. S. Han, W. A. Goddard III. *J. Am. Chem. Soc.* **129**, 8422 (2007).
40. S. Ma, J. M. Simmons, D. Sun, D. Yuan, H.-C. Zhou. *Inorg. Chem.* **48**, 5263 (2009).
41. M. Dincă, J. R. Long. *Angew. Chem., Int. Ed.* **47**, 6766 (2008).
42. S. Ma, H.-C. Zhou. *J. Am. Chem. Soc.* **128**, 11734 (2006).
43. B. Chen, N. W. Ockwig, A. R. Millward, D. S. Contreras, O. M. Yaghi. *Angew. Chem., Int. Ed.* **44**, 4745 (2005).
44. X.-S. Wang, S. Ma, P. M. Forster, D. Yuan, J. Eckert, J. J. Lopez, B. J. Murphy, J. B. Parise, H.-C. Zhou. *Angew. Chem., Int. Ed.* **47**, 7263 (2008).
45. W. Zhou, H. Wu, M. R. Hartman, T. Yildirim. *J. Phys. Chem. C* **111**, 16131 (2007).
46. A. G. Wong-Foy, A. J. Matzger, O. M. Yaghi. *J. Am. Chem. Soc.* **128**, 3494 (2006).
47. O. K. Farha, A. O. Yazaydn, I. Eryazici, C. D. Malliakas, B. G. Hauser, M. G. Kanatzidis, S. T. Nguyen, R. Q. Snurr, Joseph T. Hupp. *Nat. Chem.* **2**, 944 (2010).
48. S. K. Bhatia, A. L. Myers. *Langmuir* **22**, 1688 (2006).
49. K. L. Mulfort, J. T. Hupp. *J. Am. Chem. Soc.* **129**, 9604 (2007).
50. Y. Li, R. T. Yang. *J. Am. Chem. Soc.* **128**, 8136 (2006).
51. T. Burchell, M. Rogers. *SAE Tech. Pap. Ser.* 2000 (2000).
52. M. Kondo, T. Yoshitomi, K. Seki, H. Matsuzaka, S. Kitagawa. *Angew. Chem., Int. Ed.* **36**, 1725 (1997).
53. D. Yuan, D. Zhao, D. Sun, H.-C. Zhou. *Angew. Chem., Int. Ed.* **49**, 5357 (2010).
54. T. Düren, L. Sarkisov, O. M. Yaghi, R. Q. Snurr. *Langmuir* **20**, 2683 (2004).
55. S. Ma, D. Sun, J. M. Simmons, C. D. Collier, D. Yuan, H.-C. Zhou. *J. Am. Chem. Soc.* **130**, 1012 (2008).
56. H. Wu, W. Zhou, T. Yildirim. *J. Am. Chem. Soc.* **131**, 4995 (2009).
57. H. Wu, J. M. Simmons, Y. Liu, C. Brown, X.-S. Wang, S. Ma, V. Peterson, P. Southon, C. Kepert, H.-C. Zhou, T. Yildirim, W. Zhou. *Chem.—Eur. J.* **16**, 5205 (2010).
58. H. Kim, D. G. Samsonenko, S. Das, G. H. Kim, H. S. Lee, D. N. Dybtsev, E. A. Berdonosova, K. Kim. *Chem.—Asian J.* **4**, 886 (2009).
59. P. J. Stang, F. Diederich. *Modern Acetylene Chemistry*, VCH, New York (1995).
60. S. Budavari. *Merck Index*, Merck Research Laboratories, New Jersey (1996).
61. R. Matsuda, R. Kitaura, S. Kitagawa, Y. Kubota, R. V. Belosludov, T. C. Kobayashi, H. Sakamoto, T. Chiba, M. Takata, Y. Kawazoe, Y. Mita. *Nature* **436**, 238 (2005).
62. D. G. Samsonenko, H. Kim, Y. Sun, G.-H. Kim, H.-S. Lee, K. Kim. *Chem.—Asian J.* **2**, 484 (2007).
63. D. Tanaka, M. Higuchi, S. Horike, R. Matsuda, Y. Kinoshita, N. Yanai, S. Kitagawa. *Chem.—Asian J.* **3**, 1343 (2008).
64. S.-C. Xiang, W. Zhou, J. M. Gallegos, Y. Liu, B. Chen. *J. Am. Chem. Soc.* **131**, 12415 (2009).
65. S. Xiang, W. Zhou, Z. Zhang, M. A. Green, Y. Liu, B. Chen. *Angew. Chem., Int. Ed.* **49**, 4615 (2010).
66. N. Stern. *Stern Review on the Economics of Climate Change*, Cambridge University Press, Cambridge (2006).
67. J. Johnson. *Chem. Eng. News* **82**, 36 (2004).
68. Z. Yong, V. Mata, A. E. Rodrigues. *Sep. Purif. Technol.* **26**, 195 (2002).
69. D. M. D'Alessandro, B. Smit, J. R. Long. *Angew. Chem., Int. Ed.* **49**, 6058 (2010).
70. A. R. Millward, O. M. Yaghi. *J. Am. Chem. Soc.* **127**, 17998 (2005).
71. Y. S. Bae, O. K. Farha, J. T. Hupp, R. Q. Snurr. *J. Mater. Chem.* **19**, 2131 (2009).
72. P. L. Llewellyn, S. Bourrely, C. Serre, A. Vimont, M. Daturi, L. Hamon, G. D. Weireld, J.-S. Chang, D.-Y. Hong, Y. K. Hwang, S. H. Jung, G. Férey. *Langmuir* **24**, 7245 (2008).

73. R. Vaidhyanathan, S. S. Iremonger, K. W. Dawson, G. K. H. Shimizu. *Chem. Commun.* 5230 (2010).
74. A. Demessence, D. M. D'Alessandro, M. L. Foo, J. R. Long. *J. Am. Chem. Soc.* **131**, 8784 (2009).
75. J. An, S. J. Geib, N. L. Rosi. *J. Am. Chem. Soc.* **132**, 38 (2010).
76. R. T. Yang. *Gas Adsorption by Adsorption Processes*, Butterworth, Boston (1997).
77. J.-R. Li, R. J. Kuppler, H.-C. Zhou. *Chem. Soc. Rev.* **38**, 1477 (2009).
78. D. N. Dybtsev, H. Chun, S. H. Yoon, D. Kim, K. Kim. *J. Am. Chem. Soc.* **126**, 32 (2004).
79. S. Ma, X. S. Wang, C. D. Collier, E. S. Manis, H. C. Zhou. *Inorg. Chem.* **46**, 8499 (2007).
80. B. Chen, S. Ma, E. J. Hurtado, E. B. Lobkovsky, H.-C. Zhou. *Inorg. Chem.* **46**, 8490 (2007).
81. B. Chen, S. Ma, F. Zapata, F. R. Fronczek, E. B. Lobkovsky, H.-C. Zhou. *Inorg. Chem.* **46**, 1233 (2007).
82. S. Ma, X.-S. Wang, D. Yuan, H.-C. Zhou. *Angew. Chem., Int. Ed.* **47**, 4130 (2008).
83. S. Kitagawa, R. Kitaura, S.-i. Noro. *Angew. Chem., Int. Ed.* **43**, 2334 (2004).
84. S. Ma, D. Sun, X.-S. Wang, H.-C. Zhou. *Angew. Chem., Int. Ed.* **46**, 2458 (2007).
85. S. Ma, D. Sun, D. Yuan, X.-S. Wang, H.-C. Zhou. *J. Am. Chem. Soc.* **131**, 6445 (2009).
86. R. Hulme, R. Rosensweig, D. Ruthven. *Ind. Eng. Chem. Res.* **30**, 752 (1991).
87. L. Alaerts, C. E. A. Kirschhock, M. Maes, M. A. van der Veen, V. Finsy, A. Depla, J. A. Martens, G. V. Baron, P. A. Jacobs, J. F. M. Denayer, D. E. De Vos. *Angew. Chem., Int. Ed.* **46**, 4293 (2007).
88. S. W. Sohn. "Kerosene ISOSIV process for production of normal paraffins", in *Handbook of Petroleum Refining Processes*, 3rd ed., R. A. Meyers (Ed.), McGraw-Hill, New York (2004).
89. P. S. Barcia, F. Zapata, J. A. C. Silva, A. E. Rodrigues, B. Chen. *J. Phys. Chem. B* **111**, 6101 (2007).
90. K. Li, D. H. Olson, J. Seidel, T. J. Emge, H. Gong, H. Zeng, J. Li. *J. Am. Chem. Soc.* **131**, 10368 (2009).
91. B. Chen, C. Liang, J. Yang, D. S. Contreras, Y. L. Clancy, E. B. Lobkovsky, O. M. Yaghi, S. Dai. *Angew. Chem., Int. Ed.* **45**, 1390 (2006).
92. Z.-Y. Gu, X.-P. Yan. *Angew. Chem., Int. Ed.* **49**, 1477 (2010).
93. N. Chang, Z.-Y. Gu, X.-P. Yan. *J. Am. Chem. Soc.* **132**, 13645 (2010).
94. R. Ahmad, A. G. Wong-Foy, A. J. Matzger. *Langmuir* **25**, 11977 (2009).
95. D. Zacher, O. Shekhah, C. Woll, R. A. Fischer. *Chem. Soc. Rev.* **38**, 1418 (2009).
96. H. Guo, G. Zhu, I. J. Hewitt, S. Qiu. *J. Am. Chem. Soc.* **131**, 1646 (2009).
97. J. Y. Lee, O. K. Farha, J. Roberts, K. A. Scheidt, S. T. Nguyen, J. T. Hupp. *Chem. Soc. Rev.* **38**, 1450 (2009).
98. L. Ma, C. Abney, W. Lin. *Chem. Soc. Rev.* **38**, 1248 (2009).
99. A. Corma, H. Garcia, F. X. Llabres i Xamena. *Chem. Rev.* **110**, 4606 (2010).
100. S. Hermes, M.-K. Schröter, R. Schmid, L. Jhodeir, M. Muhler, A. Tissler, R. W. Fischer, R. A. Fischer. *Angew. Chem., Int. Ed.* **44**, 6237 (2005).
101. B. Yuan, Y. Pan, Y. Li, B. Yin, H. Jiang. *Angew. Chem., Int. Ed.* **49**, 4054 (2010).
102. M. H. Alkordi, Y. L. Liu, R. W. Larsen, J. F. Eubank, M. Eddaoudi. *J. Am. Chem. Soc.* **130**, 12639 (2008).
103. K. Schlichte, T. Kratzke, S. Kaskel. *Microporous Mesoporous Mater.* **73**, 81 (2004).
104. S. Horike, M. Dinca, K. Tamaki, J. R. Long. *J. Am. Chem. Soc.* **130**, 5854 (2008).
105. A. M. Shultz, O. K. Farha, J. T. Hupp, S. T. Nguyen. *J. Am. Chem. Soc.* **131**, 4204 (2009).
106. S. J. Garibay, Z. Wang, S. M. Cohen. *Inorg. Chem.* **49**, 8086 (2010).
107. Y. K. Hwang, D. Y. Hong, J. S. Chang, S. H. Jung, Y. K. Seo, J. Kim, A. Vimont, M. Daturi, C. Serre, G. Férey. *Angew. Chem., Int. Ed.* **47**, 4144 (2008).
108. J. S. Seo, D. Whang, H. Lee, S. I. Jun, J. Oh, Y. J. Jeon, K. Kim. *Nature* **404**, 982 (2000).
109. S.-H. Cho, B.-Q. Ma, S. T. Nguyen, J. T. Hupp, T. E. Albrecht-Schmitt. *Chem. Commun.* 2563 (2006).

110. D. N. Dybtsev, A. L. Nuzhdin, H. Chun, K. P. Bryliakov, E. P. Talsi, V. P. Fedin, K. Kim. *Angew. Chem., Int. Ed.* **45**, 916 (2006).
111. K. D. Kreuer, S. J. Paddison, E. Spohr, M. Schuster. *Chem. Rev.* **104**, 4637 (2004).
112. S. Bureekaew, S. Horike, M. Higuchi, M. Mizuno, T. Kawamura, D. Tanaka, N. Yanai, S. Kitagawa. *Nat. Mater.* **8**, 831 (2006).
113. J. A. Hurd, R. Vaidhyanathan, V. Thangadurai, C. I. Ratcliffe, I. L. Moudrakovski, G. K. H. Shimizu. *Nat. Chem.* **1**, 705 (2009).
114. M. Sadakiyo, T. Yamada, H. Kitagawa. *J. Am. Chem. Soc.* **131**, 9906 (2009).